

Dynamical nonlinearity in strained InGaAs (311)A sidewall quantum wires

Daniele Alderighi, Marian Zamfirescu, Anna Vinattieri, and Massimo Gurioli^{a)}

INFN, Department of Physics and LENS, University of Florence, Via Sansone 1, 50019,

Sesto Fiorentino, Italy

Stefano Sanguinetti

INFN and Department of Materials Science, University of Milan Bicocca, Via Cozzi 53, 20125,

Milano, Italy

Michael Povolotskyi, Jerome Gleize, Aldo Di Carlo, and Paolo Lugli

INFN, Department of Electronic Engineering, University of Rome "Tor Vergata," Roma, Italy

Richard Nötzel

eiTT/COBRA Inter-University Research Institute, Eindhoven University of Technology 5600 MB Eindhoven,

The Netherlands

(Received 4 August 2003; accepted 14 November 2003)

Significant optical nonlinearity has been found in InGaAs (311)A sidewall quantum wires by means of time resolved photoluminescence measurements. A strong reverse quantum confined Stark effect has been observed and attributed to the dynamical screening of both the internal piezoelectric field and the Coulomb interaction between carriers. The time evolution of the quantum wire emission has been reproduced by means of self-consistent calculations that take into account excitonic effects, strain, and induced piezoelectric charges. © 2004 American Institute of Physics.

[DOI: 10.1063/1.1639504]

Semiconductor quantum wires (QWRs) have been widely studied because of their peculiar electronic structure that turns out to be interesting for both fundamental physics and devices applications.¹⁻³ In order to overcome the technological bottleneck associated with the control of the nanostructure geometry not only along the epitaxial growth direction but also along the lateral directions, several growth techniques have been developed providing different kinds of QWRs with different shapes, strain patterns, structural, and electronic properties.^{1,4} The disposability of good quality QWR has stimulated studies covering a wide range of physical processes, such as, lasing action,³ transport processes,⁵ strain effects in mismatched structures on the exciton and carrier dynamics,^{1,4} kinetics of carrier recombination,^{4,6-8} and dot-wire coupling for spintronics.^{9,10} In particular, different kinds of nonlinearity are expected in semiconductor QWRs. The singularity in the density of state, due to the two-dimensional quantum confinement of the carriers, allows sharp spectral features and makes these structures extremely attractive for nonlinear optics. The discrete nature of the electronic levels, associated with the carrier confinement, produces a relevant state filling effect under large carrier injection.¹¹ At the same time, the confinement of electrons and holes in two spatial dimensions increases the exciton binding energy and therefore the effects of its screening and eventually bleaching. Enhancement of the optical nonlinearity has been found in sidewall QWRs, by means of continuous-wave photoluminescence (PL) measurements.⁷

In this article, we address the dynamics of the nonlinear optical response of sidewall QWRs grown on (311)A GaAs substrates, by means of time resolved PL (TRPL) measurements. A large dynamical quantum confined Stark effect

(QCSE) is observed in the QWRs. The quantitative comparison with a detailed microscopic model allows one to conclude that the strong optical nonlinearities are induced by the screening of the internal fields by means of carrier photoinjection.

The investigated sample has been grown by molecular-beam epitaxy on a patterned GaAs (311)A substrate processed into shallow mesa stripes 10 μm wide and 20 nm deep along [01-1] by optical lithography and wet chemical etching. The sample structure grown on this substrate is comprised of the following layer sequence: 50 nm GaAs buffer layer followed by a 50 nm thick $\text{Al}_{0.5}\text{Ga}_{0.5}\text{As}$ barrier layer. After the deposition of the 3 nm thick active $\text{In}_{0.2}\text{Ga}_{0.8}\text{As}$ layer, again, a 50 nm thick $\text{Al}_{0.5}\text{Ga}_{0.5}\text{As}$ barrier and a 10 nm GaAs cap layer have been grown. The QWRs are formed spontaneously during the growth at the sidewall by the migration of InGaAs from the flat adjacent quantum wells (QW) regions. In the following, we will present a series of TRPL measurements obtained after nonresonant excitation ($\hbar\omega_{\text{exc}}=3.5$ eV) by the second-harmonic generation of a ps Ti:Sapphire laser. The PL signal was detected in backscattering configuration and spectrally analyzed by a 1/4 m monochromator with spectral resolution of ~ 1 nm. Time resolved spectra were acquired by means of a Streak Camera with time resolution better than 10 ps.

In Fig. 1(a), a time-energy PL pattern at $T=10$ K is shown. Two PL bands are present corresponding to the QW (higher-energy) and QWR (lower-energy) emission. The continuous white lines on the picture mark the maximum of the PL bands of the QW and QWR. At short time delay after the pulse excitation, the QWR and QW emission tend to merge due to the broadening on the high-energy side of the QWR PL band. Increasing the time delay, the two bands shift toward lower energies and become well separated. It is impor-

^{a)}Electronic mail: gurioli@fi.infn.it

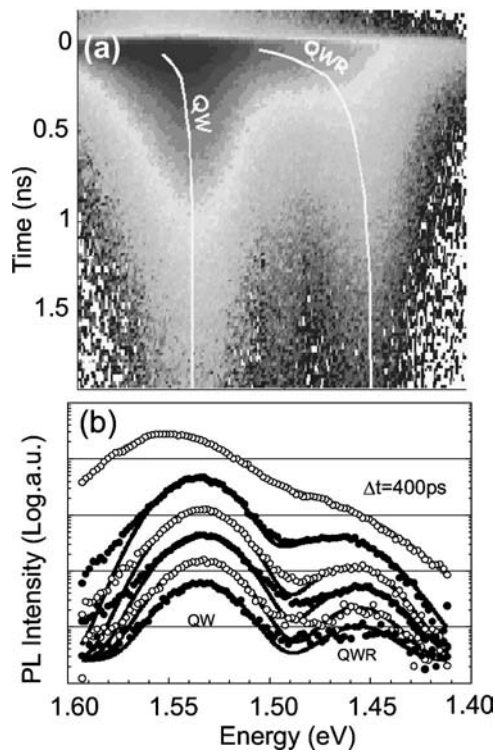


FIG. 1. (a) PL log pattern vs energy and time. The white lines show the redshift of the maximum of the PL bands of the QW and QWR emission. (b) Experimental data (circles) and Gaussian fits (lines) of the TRPL spectra extracted from the time-energy pattern shown in (a).

tant to note that the time-energy PL pattern, observed when reducing the excitation power, is exactly the same, within the experimental errors, as that for long time delays. Hence, the PL time evolution is completely determined by the carrier injected in the nanostructures. TRPL spectra can be extracted from the time-energy pattern of Fig. 1 by horizontally cutting the PL map for various time delays and by averaging over a time window of 30 ps. We have fitted the PL spectra by using two Gaussian curves in order to separate the QW and QWR contributions. The experimental data (circles) and the fitting curves (lines) are shown in Fig. 1(b) with a time separation of $\Delta t = 400$ ps, starting from the spectrum at zero delay. In case of short time delays, the QW and QWR PL bands are merged due to the broadening on the high-energy side of the QWR PL band. This is very likely associated with the QWR state filling of the high-energy excited states,¹¹ even if the presence of other many-body effects cannot be excluded. The strong overlap of the QW and QWR PL bands does not allow a careful estimation the energy of the fundamental transitions. The overlap of the two PL bands is overcome after nearly 300 ps when a clear dip in the PL spectrum appears in between the QW and QWR emission. Therefore, after nearly 300 ps, the PL peak positions, extracted by Gaussian fits, can be safely associated with the fundamental transition energy which redshifts with increasing time delay as a consequence of the photoinduced screening.

In order to interpret the experimental data, we have developed a theoretical model for calculating the electronic structure of the QWR. The elastic deformation of the structure is calculated by means of a continuum mechanical model,¹²⁻¹⁴ taking into account boundary conditions for high Miller index crystal planes.^{15,16} Then, the piezoelectric polar-

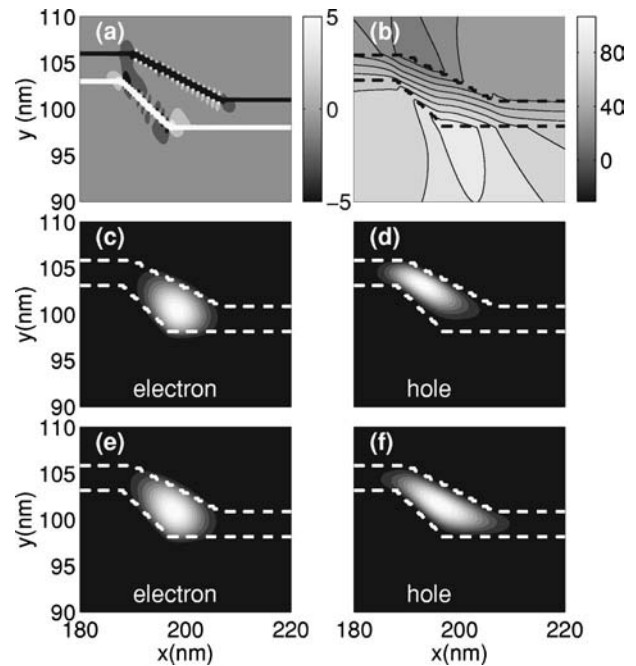


FIG. 2. (a) Cross-sectional contour plots of the piezoelectric charge density; the units of the color bar are $10^{18} e \text{ cm}^{-3}$. (b) Cross-sectional contour plots of the electric potential; the units of the color bar are mV. (c)–(f) Squared modulus of the single-particle wave function for the ground state of electron and hole. (c) and (d) correspond to the case when the field is not screened. (e) and (f) correspond to the case of full field screening. In (b)–(f), the dashed lines indicate the barrier interfaces.

ization \mathbf{P}_p is determined as a linear function of the strain tensor: $P_i = e_{ijk} \epsilon_{jk}$. The piezoelectric charge density $\rho(\mathbf{r}) = -\text{div} \mathbf{P}_p(\mathbf{r})$ is plotted in Fig. 2(a). There are two different charge contributions: Surface charge at the interfaces due to the discontinuity of the polarization vector and volume charge induced by the nonhomogeneous strain. The first contribution is a peculiarity of structures grown on [N11] oriented substrates. The volume charge is concentrated near both material sidewalls with positive and negative contributions at opposite sides. The electric potential due to the piezoelectric charge is shown in Fig. 2(b). In the QW region, far from the wire, the electric field is parallel to the growth direction and equal to 90 kV/cm. In the QWR, the electric field is nonhomogeneous and has a nonzero component perpendicular to the growth direction. In order to calculate the electronic states, we use the effective-mass approximation to describe electrons in the conduction band and holes in the valence band. We consider the heavy hole only, with anisotropic effective mass that depends on strain. The strain-induced shift of the conduction band depends only on the hydrostatic part of the strain: $\delta E_c = -a_c \text{Tr}(\epsilon_{ij})$. Band shifts and effective-mass tensors for the three upper valence bands are obtained from the Bir-Pikus 6×6 Hamiltonian.^{17,18}

The theoretical predictions can be directly compared with the experimental data at long time delay, or low carrier injection (parameters for the calculations were taken from Ref. 19). In the case of large carrier band filling, various many-body effects can occur and a quantitative description becomes very complicated; therefore, we skip the large carrier injection condition and consider only the regime of the carrier recombination kinetics where the fundamental optical transitions are shifted due to the carrier screening. Assuming

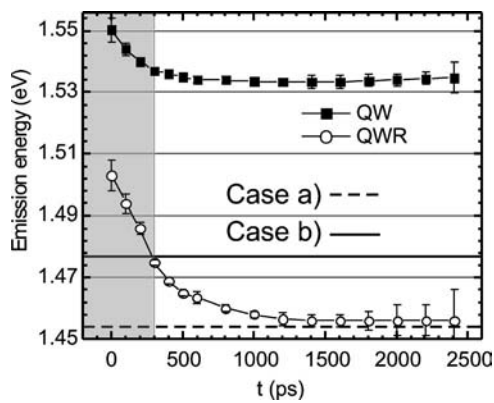


FIG. 3. Extracted peaks position of the TRPL spectra shown in Fig. 1(b). The gray area refers to the time interval where large overlap of the PL bands is observed. Horizontal dashed and solid lines represent the calculated values for the cases a) and b), respectively.

a complete screening of the piezoelectric field and the carrier Coulomb interaction, this latter effect can be accounted for by calculating the variation of the QWR optical transition energy and oscillator strength by switching off the piezoelectric potential. Modules squared of the electron and hole wave functions are shown in Figs. 2(c)–2(f) for the two extreme cases: Case a [Figs. 2(c)–2(d)], when the concentration of free charges is negligible, that the piezoelectric field is present, and case b [Figs. 2(e)–2(f)], when the built-in field is completely screened by nonequilibrium charge carriers. In case a, a large electron–hole separation due to the piezoelectric field can be observed. Finally, in the low injection limit (case a), we have to consider excitonic effects. The effect of Coulomb attraction between electrons and holes cannot be neglected since it is comparable to the effect of the carrier separation due to the piezoelectric field. Hence, electron (hole) wave functions of the ground state ψ_e^0 (ψ_h^0) are considerably perturbed by the excitonic effect. This perturbation is taken into account in the framework of our variational approach.^{20,21} In case b, the electron–hole Coulomb interaction is screened by the large carrier injection.

The comparison between experimental data and theoretical predictions is presented in Fig. 3; the gray area represents the time interval where a strong overlap of the PL bands is observed. For the sake of completeness, we report in Fig. 3, the energy positions obtained by the two Gaussians fit also for the gray area, even if, in such a case, these data do not represent the fundamental optical transitions. A safe evaluation of the fundamental optical transition can be obtained only for time delays longer than 300 ps. For the QW, the residual PL shift is only ≈ 4 meV, while for the QWR, the redshift is much larger (≈ 20 meV). The horizontal dashed and solid lines in Fig. 3 represent the QWR theoretical predictions for the two limiting cases a and b, respectively. The shift of the QWR optical transition is predicted to be the order of 22 meV. Obviously, our experimental estimate of the energy shift of the fundamental optical transition (≈ 20 meV) is only a lower limit of the total shift. Still, the

agreement with the theory is rather good and allows us to attribute the PL optical nonlinearity to the reversed QCSE, due to the screening of the internal field by the photoinduced carriers. The much larger shift observed in the QWR with respect to the QW is connected with the larger electron–hole separation occurring in the QWR with respect to the QW. As a final test of the consistency of our attribution, we evaluate the oscillator strength of the interband optical dipole transition in the two limiting cases, a and b. We find that the electron–hole separation induced by the piezoelectric field gives rise to a reduction of the oscillator strength of a factor of 2 which is fully consistent with the experimental data.

In conclusion, we have investigated the dynamical optical nonlinearity of strained InGaAs sidewall QWRs on patterned GaAs substrates. The experimental results quantitatively agreed with the theoretical predictions based on self-consistent calculations. We demonstrate that the large dynamical QCSE observed in the QWRs arises from the screening of the internal fields by means of carrier photoinjection. We find that both the piezoelectric fields and electron–hole Coulomb interaction have to be considered in order reproduce the experimental findings.

This work was partially supported by the European Community under Contract Nos. HPRICT 1999-000111 and HPRN-CT-1999-00132. One of the authors (M.P.) acknowledges support by the INFM PA-PIE project.

- ¹C. Constantin, E. Martinet, F. Lelarge, K. Leifer, A. Rudra, and E. Kapon, *J. Appl. Phys.* **88**, 141 (2000).
- ²H. Weman, M.-A. Dupertuis, E. Martinet, A. Rudra, and E. Kapon, *Appl. Phys. Lett.* **79**, 4 (2001).
- ³L. Sirigu, D. Y. Oberli, L. Degiorgi, A. Rudra, and E. Kapon, *Phys. Rev. B* **61**, 16 (2000).
- ⁴R. Nötzel, M. Ramsteiner, Z. Niu, L. Däweritz, and K. H. Ploog, *Physica E (Amsterdam)* **2**, 979 (1998).
- ⁵U. Jahn, R. Nötzel, J. Ringling, H.-P. Schönherr, H. T. Grahn, and K. H. Ploog, *Phys. Rev. B* **60**, 11038 (1999).
- ⁶K.-J. Friedland, H.-P. Schönherr, R. Nötzel, and K. H. Ploog, *Phys. Rev. Lett.* **83**, 156 (1999).
- ⁷R. Nötzel, J. Menniger, M. Ramsteiner, A. Ruiz, H.-P. Schönherr, and K. H. Ploog, *Appl. Phys. Lett.* **68**, 1132 (1996).
- ⁸M. Lomascolo, P. Ciccarese, R. Cingolani, R. Rinaldi, and F. K. Reinhardt, *J. Appl. Phys.* **83**, 302 (1998).
- ⁹T. Rejec, A. Ramsak, and J. H. Jefferson, *Phys. Rev. B* **62**, 12985 (2000).
- ¹⁰M. A. Davidovich, E. V. Anda, and C. A. Büsser, *Phys. Rev. B* **65**, 233310 (2002).
- ¹¹W. R. Tribe, M. J. Steer, D. J. Mowbray, M. S. Skolnick, A. N. Forshaw, J. S. Roberts, G. Hill, M. A. Pate, C. R. Whitehouse, and G. M. Williams, *Appl. Phys. Lett.* **70**, 993 (1997).
- ¹²C. Pryor, M. E. Pistol, and L. Samuelson, *Phys. Rev. B* **56**, 10404 (1997).
- ¹³B. Jogai, *J. Appl. Phys.* **88**, 5050 (2000).
- ¹⁴Nextnano³ device simulation package, see web site url <http://www.nextnano.de>
- ¹⁵E. Anastassakis, *J. Appl. Phys.* **68**, 4561 (1990).
- ¹⁶L. De Caro and L. Tapfer, *Phys. Rev. B* **48**, 2298 (1993).
- ¹⁷C. Y.-P. Chao and S. L. Chuang, *Phys. Rev. B* **46**, 4110 (1992).
- ¹⁸R. H. Henderson and E. Towe, *J. Appl. Phys.* **78**, 2447 (1995).
- ¹⁹I. Vurgaftman, J. R. Meyer, and L. R. Ram-Mohan, *J. Appl. Phys.* **89**, 5815 (2001).
- ²⁰A. A. Kiselev and U. Rössler, *Semicond. Sci. Technol.* **11**, 203 (1995).
- ²¹F. L. Madarasz, F. Szmulowicz, F. K. Hopkins, and D. L. Dorsey, *Phys. Rev. B* **49**, 13528 (1994).